# Experimental and numerical simulation of the wall-pressure fluctuation on the isolated helicopter fuselage

*Andrei* Batrakov[1,*]

[1]Researcher, Aerodynamics Department, 420111 K. Marx street 10, Kazan, Russia

**Abstract.** This work is devoted to wall-pressure fluctuation analysis. The object of investigation was an isolated helicopter fuselage. Investigation was carried out by experimental and numerical methods. Numerical simulation was based on RANS and DES approaches. The experiment was carried out in a low-speed wind tunnel with an open test section. Wall-pressure fluctuation was measurement by high-frequency pressure probes ENDEVCO 8510B-2. The experimental results were compared with both DES data and results by the semi-empirical model based on the RANS simulation. It was shown that DES modelling provides a wall-pressure spectrum for low and middle-frequency parts. For simulation high-frequency part of the spectrum, the semi-empirical model is preferable.

## 1 Introduction

In recent years the helicopter aeroacoustics is of great interest to researchers. The actuality of this research field is due to increased requirements for the helicopters. The main trend of requirements is the decreasing of the noise emission and improvement of flight comfort. These tasks have especially relevant to the development of the advanced high-speed aircraft.

Helicopter has different noise sources that are characterized by amplitude, frequency range and radiation direction. The main helicopter noise sources are the main and the tail rotors, the transmission (gearbox), the engine and the turbulent boundary layer. According to the radiation direction of the acoustic field can be separated into the interior and the exterior parts. For interior noise, the most important frequencies are related to the 500 Hz – 4 kHz range due to the human ear sensitivity. The typical acoustic signature inside the helicopter cabin presented in Figure 1 consists of tonal noise from the main gearbox and the engines and the broadband noise from aerodynamic excitation.

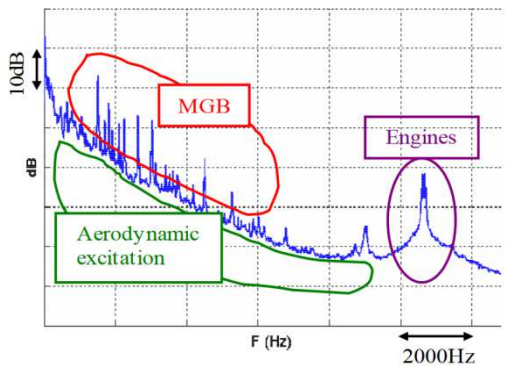


**Fig. 1.** Power spectral density of helicopter interior noise [1].

The tonal noise from gearbox and engines has a structure-borne path and can be reduced by active or passive vibration dumping. The aerodynamic excitation noise reaches into the helicopter cabin crossing the fuselage skin and windows. Recent studies proposal a new helicopter trim panel with high acoustic transmission loss [2]. Development material with high acoustic transmission loss for helicopter windows is very difficult task. Anyway, the accurate prediction of the interior noise is a very actual problem. For this goal, it is necessary to evaluate the parameters of the aeroacoustics sources, in particular, the wall-pressure fluctuation due to the turbulent boundary layer.

Evaluation of the turbulent wall-pressure fluctuation can be performed by different approaches like direct numerical simulation of pressure fluctuation or using models based on auto-spectral/cross-spectral analysis.

The present paper focuses on the prediction of the wall-pressure fluctuation on the isolated helicopter fuselage. Investigation is carried outed by both experimental and numerical approaches.

## 2 Experimental approach

The experimental investigation is carried out by the open test section closed-circuit low-speed T-1K wind tunnel of Kazan National Research Technical University (KNRTU). The diameter of the test section is 2.25m. The wind tunnel can be operated at wind speeds up to 50 m/s and it has freestream turbulence intensity below 0.5% in the jet core. Science 2014 year the wind tunnel has equipped by anechoic chamber as it presented in Figure 2.

The object of investigation is the model of helicopter fuselage that is presented in Figure 3. The considered model of the fuselage is the prototype of the multi-

* Corresponding author: asbatrakov@kai.ru

proposal helicopter ANSAT produced by Kazan Helicopter Plant.

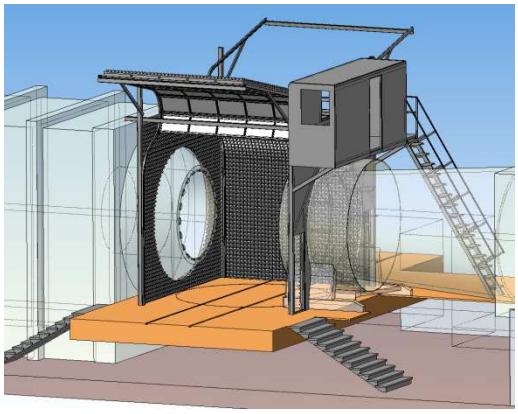

**Fig. 2.** Wind tunnel with anechoic chamber.

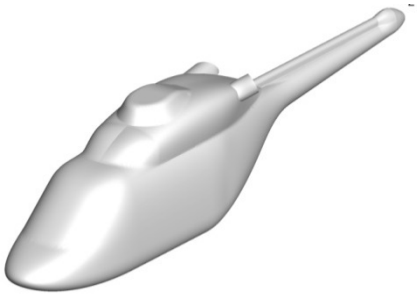

**Fig. 3.** The isolated fuselage model.

The wind tunnel model has a fuselage length of 1.8 m, and a reference area of $S_F$= 0.106 m$^2$. At the previous work [3] the integral aerodynamic characteristics of the model were analysed by experiment and numerical simulation.

Investigation of the pressure fluctuation was carried out at the following flow conditions: Mach number is M=0.1 and Reynolds number is Re=4.4·10$^6$. For the wall-pressure measurement, the fuselage model was equipped by high-frequency pressure probes ENDEVCO 8510B-2. Due to probes are differential types it is necessary to have a reference pressure tube. To get more information during the experiment the model was equipped by accelerometer. The equipment layout is presented in Figure 4.

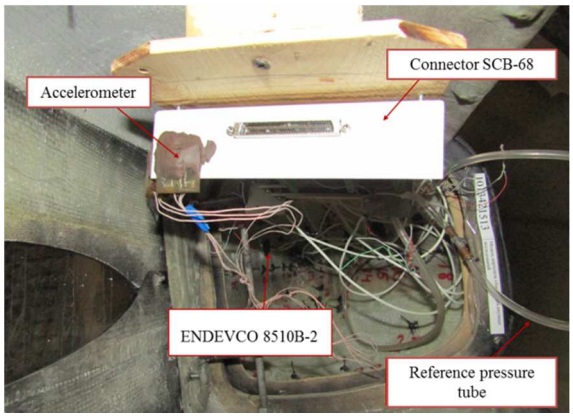


**Fig. 4.** Equipment inside the fuselage.

The power supply and data wires with the reference pressure tube were routed through the hole near the rotor head. The fuselage was mounted by six-component Prandtl-type balance as it is presented in Figure 5.

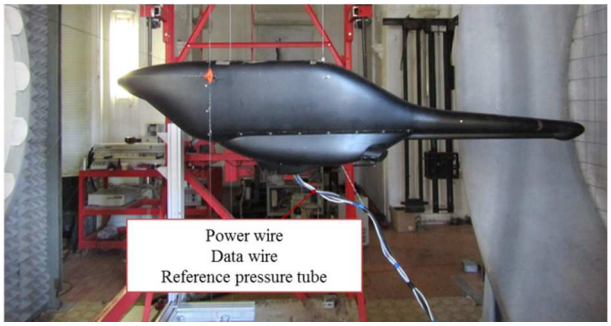


**Fig. 5.** The mounting of the fuselage model.

The high-frequency pressure probes were distributed on the fuselage surface as it is illustrated in Figure 6 to focus on the front and rear parts of the fuselage.

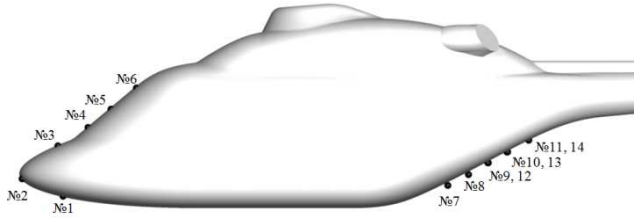


**Fig. 6.** High-frequency pressure probes location.

## 3 Numerical approach

The numerical simulation was carried out using the in-house CFD code Helicopter Multi-Block (HMB). Some details of this CFD code are presented in [4]. The solver provides a Reynolds averaged Navier – Stokes simulation (RANS/URANS) with different turbulence models as well as the hybrid approaches like a scale adaptive simulation (SAS), detached eddy simulation (DES) and large eddy simulation (LES). Investigation of the averaged flow characteristics was based on the RANS simulation with the $k$-$\omega$ SST turbulence model. Unsteady pressure was evaluated by DES approach.

For the spatial discretization of Navier Stokes equations, the ANSYS ICEM Hexa-mesh generation tool has been used. The computational grid has a multi-block topology. The O-grid type of topology with the high resolution is used near the fuselage to resolve surface boundary layers (Figure 7). The full grid consists of 964 blocks. The number of cells and parameters of cells distribution were determined by the study of grid independence [3, 5]. As a result, the spacing of the near-wall grid in the normal to surface direction was 1·10$^{-5}$ of the fuselage length, the cells size ratio was 1.2, and the total number of cells was 13.5·10$^6$.

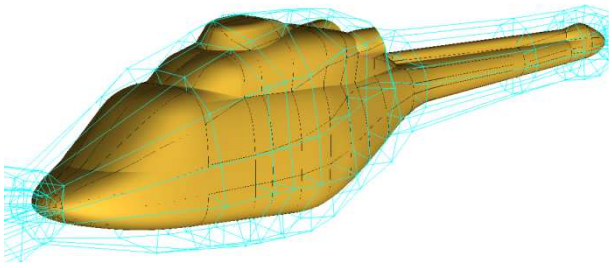

**Fig. 7.** Mesh topology near the fuselage.

### 3.1 Wall-pressure fluctuation model

The wall-pressure fluctuation can be evaluated by the semi-empirical model. Recent studies proposal different models, which are trim to the different experimental data. One of famed model was proposed by Goody [6]. This model is used as a start point by many works [7-10] with the aim to extend the range of application including non-zero gradient pressure.

The original Goody model (1) uses aerodynamic quantities like the local boundary layer thickness $\delta_l$, the boundary layer edge velocity $U_e$, the wall shear stress $\tau_\omega$ and the friction velocity $U_\tau$

$$\frac{\Phi(\omega)U_e}{\tau_\omega^2\delta_l} = \frac{a\left(\frac{\omega\delta_l}{U_e}\right)^b}{\left[\left(\frac{\omega\delta_l}{U_e}\right)^c + d\right]^e + \left[fR_T^g\left(\frac{\omega\delta_l}{U_e}\right)\right]^h}, \quad (1)$$

where

$$R_T = \frac{U_\tau^2\delta_l}{U_e\nu}, \qquad U_\tau = \sqrt{\frac{\tau_\omega}{\rho}}. \quad (2)$$

Parameters $a$ – $h$ in the original model are constant coefficients presented in Table 1.

**Table 1.** Parameters of Goody model.

| $a$ | $b$ | $c$ | $d$ | $e$ | $f$ | $g$ | $h$ |
|---|---|---|---|---|---|---|---|
| 3.0 | 2.0 | 0.75 | 0.5 | 3.7 | 1.1 | -0.57 | 7 |

Other models keep the main form of equation 1 but propose to use different aerodynamic parameters like the boundary layer displacement thickness $\delta_*$, the boundary layer momentum thickness $\theta$, the boundary layer shape factor H, velocity and dynamic pressure of the freestream. To increase the model flexibility some parameters from $a$ to $h$ are represented as a function of Reynolds number. To take into account non-zero pressure gradient conditions Cole's wake parameter [11] with Clauser's equilibrium parameter [12] can be introduced to the model.

The combination of wall-pressure fluctuation model with numerical simulation based on RANS seems very promising. This approach allows analysing pressure spectrum with a relatively low computational cost. However, some parameters of the model are difficult to determine with high accuracy by CFD results, especially for the complex objects. For example, the boundary layer thickness defined as the distance from surface to location at 99% of the freestream velocity is difficult to use.

On the other hand, the main reason for the wall-pressure fluctuation is the turbulence inside the boundary layer. RANS simulation allows evaluating averaged parameters of the turbulence like as kinetic energy ($k$) and specified kinetic energy dissipation rate ($\omega_t$). For example, Klabes et. al. [13] proposes to use kinetic energy instead of wall shear stress.

In present work is proposed to use the characteristic source frequency $\omega_0$ as the frequency scale. The characteristic source frequency can be evaluated by the Strouhal relation for the turbulent flow [14]:

$$\frac{\omega_0 l_0}{u_o} \approx 1.7. \quad (3)$$

Characteristic length $l_0$ and velocity scale $u_o$ for the turbulence can be determined at the point of the boundary layer with a maximum of kinetic energy:

$$u_o = \max\left(\sqrt{k(y)}\right) = \sqrt{k(y_{max})}, \quad 0 \le y \le \delta_l \quad (4)$$

$$l_0 = \frac{u_o}{\omega_t(y_{max})} \quad (5)$$

Taking into account these assumptions it is seen that the characteristic source frequency $\omega_0$ proportional to the specified kinetic energy dissipation rate $\omega_t$.Thus, the wall-pressure spectrum model is rewritten as:

$$\Phi(\omega) = \frac{\rho^2 k(y_{max})^2}{\omega_0} \frac{a\left(\frac{\omega}{\omega_0}\right)^b}{\left[\left(\frac{\omega}{\omega_0}\right)^c + d\right]^e + \left[fRe_t^g\left(\frac{\omega}{\omega_0}\right)\right]^h}, \quad (6)$$

where $Re_T$ is the turbulent Reynolds number.

$$Re_t = \frac{k(y_{max})}{\omega_t(y_{max})\nu}. \quad (7)$$

To determine the model parameters the test case form [8] was considered. The test case represents the flow around the flat plate. The turbulent parameters of the boundary layer were obtained by the RANS simulation. Numerical simulation was carried outed in two-dimensional mode. Computational domain is presented in Figure 8.

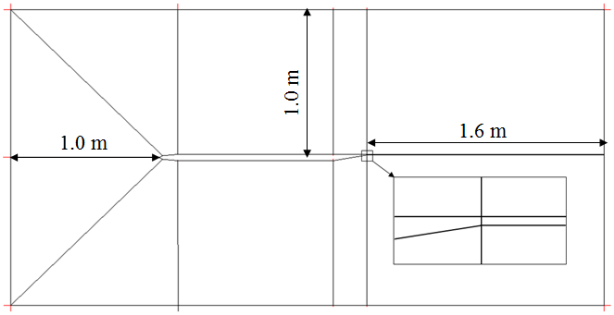


**Fig. 8.** Flat plate test case.

CFD data were compared with experiment in terms of boundary layer parameters at the control point (x=1210 mm from the leading edge). The results are presented in Table 2.

**Table 2.** Boundary layer parameters.

| | $\delta_l$ (mm) | $\delta_*$ (mm) | $\theta$ (mm) | H |
|---|---|---|---|---|
| Experiment | 19.7 | 3.51 | 2.49 | 1.41 |
| CFD | 19.7 | 3.25 | 2.42 | 1.34 |
| | $U_\tau$ | $Re_x$ | $Re_\tau$ | $Re_\theta$ |
| Experiment | 1.125 | $2.4 \cdot 10^6$ | 1439 | 4889 |
| CFD | 1.123 | $2.4 \cdot 10^6$ | 1504 | 4971 |

According to the data from the Table 2, the numerical results have a good agreement with experiment. Based on these parameters the power spectral density was calculated by the model presented at [8] (Figure 9).

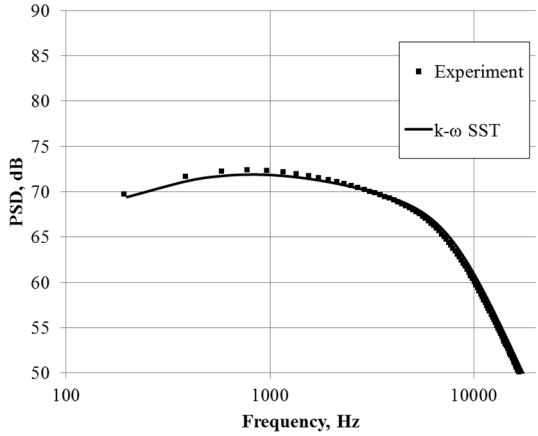


**Fig. 9.** Power spectral density at the control point.

In order to ensure greater consistency models, four points along the flat plate were considered. The power spectral density at these points was calculated by model [8] based on the boundary layer parameters and by proposal model based on the turbulent parameters of the near-wall flow. Results are presented in Figure10.

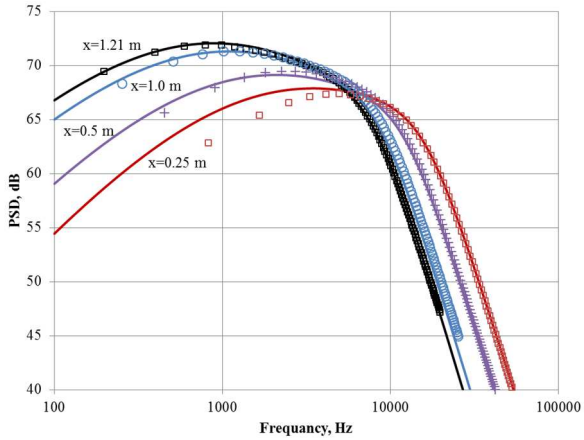


**Fig. 10.** Power spectral density at the points along the flat plate. Solids lines – current model, symbols – model [8].

Presented in Figure 10 results by the current model were obtained using the coefficients are presented in Table 3.

**Table 3.** Parameters of the current model.

| *a* | *b* | *c* | *d* | *e* | *f* | *g* | *h* |
|---|---|---|---|---|---|---|---|
| 1.3 | $f(Re_t)$ | 0.75 | 0.2 | 4 | 2 | -0.18 | 6.7 |

Here

$$b = 3.6 - Re_t^{0.21}. \quad (8)$$

## 4 Results and discussions

At this paper, the analyzing of results focuses on the two pressure probes at the front part (№1, №4) and the two pressure probes at the rear part of the fuselage ( №8 and №11). The power spectral density of the pressure based on the experimental data is presented in Figure 11.

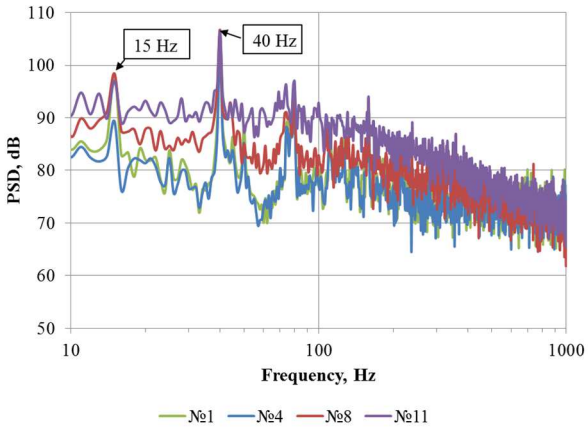


**Fig. 11.** Experimental PSD of the wall-pressure.

The Figure 11 shows that the position along the fuselage of the probe significant influences on the pressure power spectral density The pressure PSD at the lower frequency range is increased due to increasing of the X position along the fuselage. The spectral analysis shows that there are two peaks at the frequencies 15 Hz and 40 Hz. The first peak at the 15 Hz is observed due to the freestream flow characteristics in the wind tunnel. This assumption was confirmed by analysis of the velocity spectrum. The freestream velocity was measurement by the Constant Temperature Anemometry (CTA) system. The CTA transducer was located in front of the fuselage as it is presented in Figure 12.


**Fig. 12.** Locations of the CTA transducer.

As a result, it can be concluded that the first peak at the 15 Hz frequency is not related to the turbulent boundary pressure fluctuation. This frequency also is observed in the spectrum of the accelerometer signal.

The second characteristic peak at frequency 40 Hz (and the double frequency 80 Hz) perhaps relate to the natural frequency of the fuselage mounting system. This assumption needs further investigation.

The numerical data based on the DES-simulation presented in Figure 13. The DES simulation was carried out with time step $5 \cdot 10^{-5}$s. At the front point, the pressure spectrum has a very low power that relates to a very thin boundary layer and idealized conditions of numerical simulation.

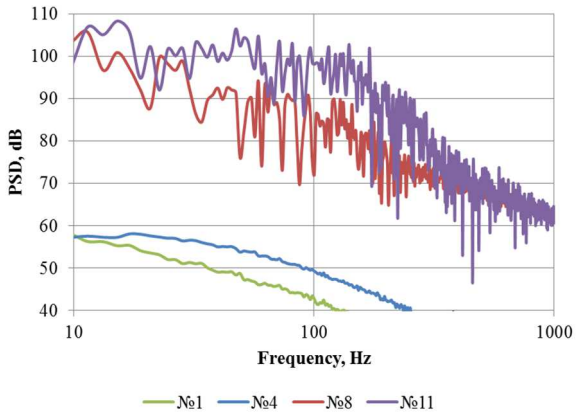


**Fig. 13.** PSD of the wall-pressure based on the DES model.

At the rear part of the fuselage, the flow is characterized by complex vortex structure [15], that provides enough strong wall-pressure fluctuation.

The PSD of the pressure fluctuation also was calculated by the proposal at the current paper model based on the RANS simulation. The results of the calculation are presented in Figure 14.

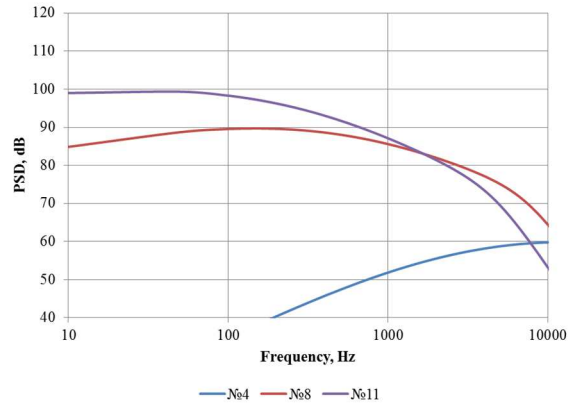


**Fig. 14.** PSD of the wall-pressure based on the proposed model.

The numerical simulation data for the rear part of the fuselage were compared with experiment. The result of comparison is presented in Figure 15 and 16.

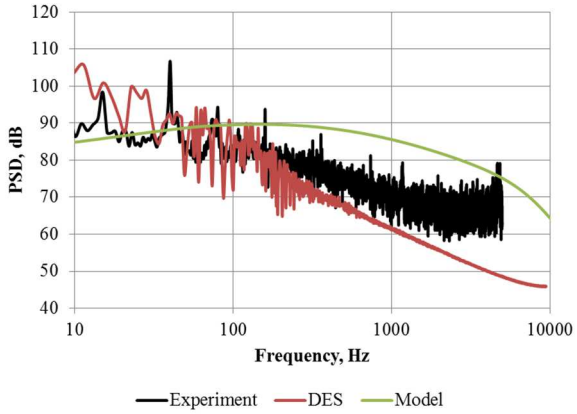


**Fig. 15.** Comparison of PSD at point №8 based on the different approaches.

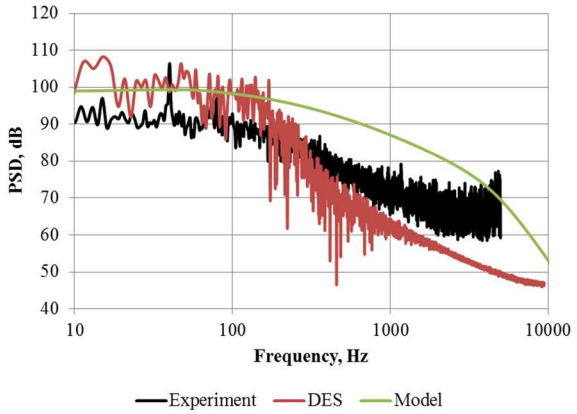


**Fig. 16.** Comparison of PSD at point №11 based on the different approaches.

As it is shown the DES simulation data have some agreement with experiment at low-frequency range up to 200…500 Hz. At the high-frequency range, the DES simulation data show fast descent of power spectral density. The proposal model overestimates the PSD at the high-frequency range. Both numerical approaches didn't show any peaks at the characteristic frequency in contradistinction to the experiment.

## 5 Conclusion

This paper presents results of experimental and numerical estimation of the wall-pressure fluctuation on the helicopter fuselage. Analysis of the experimental data shows that parameters of the wind tunnel and mounting system influence on the results. Further research will be devoted to development filter to extract pressure fluctuation due to only the turbulent boundary layer. The DES approach allows estimate wall-pressure fluctuation, but high spectrum resolution requires a high computational cost. The proposed model of the wall-pressure PSD based on the RANS simulation seems attractive to use, but this model needs further investigation to improve accuracy and to expand the operating range.

This work was supported by the grant from the Russian Science Foundation (project № 18-79-00318).

## References

1. J. Caillet, F. Marrot, F. Malburet, J-C. Carmona, 31st European Rotorcraft Forum, 13-15, September 2005, Florence, Italy (2005).
2. J. Derr´e, F. Simon, 42nd European Rotorcraft Forum, 5-8, September 2016, Lille, France (2016).
3. A. Batrakov, L. Garipova, A. Kusyumov, S. Mikhailov, G. Barakos, Journal of Aircraft, **52**(5), 1634–1643, (2015).
4. S. Lawson, G. N. Barakos, *Progress in Aerospace Sciences*, **47** (3), 186–216, (2011).
5. A.S. Batrakov, A.N. Kusyumov, S.A. Mikhailov, G.N. Barakos, Aerospace Science and Technology, 77, 704–712, (2018).
6. M. Goody, AIAA Journal, **42** (9), 1788–1794, (2004).
7. Y. Rozenberg, G. Robert, S. Moreau, AIAA Journal, **50** (10), 2168-2179, (2012).
8. N. Hu, M. Herr, Aeroacoustics Conferences, 30 May – 1 June, Lyon, France (2016).
9. M. Kamruzzaman, D. Bekiropoulos, T. Lutz, W. Würz, International journal of aeroacoustics, **14,** 833–882, (2015).
10. M. R. Catlett, J. M. Anderson, J. B. Forest, D. O. Stewart, AIAA Journal, **54** (2), 569-587 (2016).
11. D. Cole, J. Fluid Mech., **1** (2), 191-226, (1956).
12. F. H. Clauser, Journal of the Aeronautical Sciences, **21**(2), 91–108, (1954).
13. A. Klabes, C. Appel, M. Herr, S. Callsen. Inter-Noise, Hamburg, Germany, (2016).
14. G. M. Lilley. Journal of Sound and Vibration, **239**(4), 849-859, (2001).
15. A. S. Batrakov, A. N. Kusyumov, S. A. Mikhailov, L. I. Garipova, G. N. Barakos, 40th European Rotorcraft Forum, 2-5, September 2015, Southampton, UK, (2014).